

Magnetic and Electronic Properties of γ -Fe and γ -Fe/Al Particles in Copper

*Diana Guenzburger and D.E. Ellis**

Centro Brasileiro de Pesquisas Físicas - CBPF
Rua Dr. Xavier Sigaud, 150
22.290-180 Rio de Janeiro/RJ, Brasil

*Department of Physics and Astronomy
and Materials Research Center
Evanston, IL 60208, U.S.A.

ABSTRACT

The local density Discrete Variational method was employed to study the electronic structure and magnetic properties of ferromagnetic (FM) and antiferromagnetic (AFM) γ -Fe, represented by a 62-atom embedded cluster of cubic geometry, and of an iron particle in a copper matrix, represented by the cubic embedded cluster $\text{Fe}_{14}\text{Cu}_{48}$. It was found that the Cu 3d magnetic moments are aligned parallel to the Fe 3d moments, whereas the Cu(4s,4p) moments are aligned antiparallel, in agreement with recent experiments on multilayers. The influence of substitutional Al in γ -Fe and in the Fe particle in Cu was assessed. It was found that the presence of an Al impurity disrupts the AFM state locally. Magnetic hyperfine fields were calculated in all cases for comparison with Mössbauer data.

Key-words: γ -Fe; Magnetic; Electronic.

I Introduction

In the last decade there has been a revived interest in the properties of fcc (or γ) Fe, which when pure exists only at very high temperatures (between 1183 and 1667K). The existence of multiple magnetic states, the relative stability of which depends critically on the lattice constant, has been demonstrated by band structure calculations [1], [2], and may be related to the properties of γ -Fe-based INVAR alloys [3]. γ -Fe is of further technological interest since it forms the basis of austenite-type steels, where it is stabilized at low temperatures by the presence of interstitial carbon and other (transition metal) impurities. γ -Fe may be stabilized at low temperatures as small coherent precipitates in copper or copper alloy matrices [4]-[11] or as thin epitaxial films on a Cu or Cu-based alloy substrate [12], [13]. Such techniques are quite valuable, inasmuch as they allow the investigation of γ -Fe at lower temperatures with probes such as neutron diffraction and Mössbauer spectroscopy; however, it is obvious that the atoms of the matrix or substrate will induce changes in the electronic and magnetic properties of the metal. To determine these changes, first-principles electronic structure calculations may be very useful.

In the case of systems with two-dimensional translation symmetry, fcc Fe overlayers or sandwiches with Cu have been investigated with the FLAPW (full potential linearized augmented plane wave) method [14] in k-space. As for γ -Fe precipitates in Cu, models may be conveniently constructed and treated with a first-principles embedded cluster method in real space. Such methods, which consider a group of atoms to simulate the environment in a solid, are in fact ideally tailored to treat small particles of a metal in a host matrix, a system that would require a very large supercell in theories that rely on translational symmetry.

In this paper we report first principles electronic structure cluster calculations for fcc iron particles in copper. In section II we describe briefly the theoretical method, in section III we present and discuss the results and in section IV we summarize our conclusions.

II Theoretical Method

We employed the Discrete Variational method (DVM) in the framework of local density theory, which has been extensively described in the literature [15]-[17]. The DV method has been applied successfully to study magnetic, hyperfine and structural properties of numerous metallic systems [18]-[21]. A cluster of 62 atoms in cubic geometry (see Fig. 1) was considered to represent Fe in the fcc crystal structure, as well as a coherent particle of Fe in an fcc Cu matrix. In the latter case, the Fe particle is constituted by the innermost 14 atoms of the cube, and is surrounded by 48 copper atoms situated on the cube faces (see Fig. 2). The cubic cluster is embedded in the charge density of several shells of atoms (Fe or Cu) of the external part of the crystal, obtained by numerical atomic local density calculations [22]. The external charge density that penetrates the cluster region is added to the cluster density, in the construction of the Kohn-Sham hamiltonian. This is given by (in atomic units):

$$(-\nabla^2/2 + V_c + V_{xc}^\sigma)\phi_{i\sigma} = \epsilon_{i\sigma}\phi_{i\sigma} \quad (1)$$

where V_c is the Coulomb potential (nuclear and electronic) and V_{xc}^σ is the local exchange-correlation potential as given by von Barth and Hedin [23]. The cluster spin density for each spin σ is defined by

$$\rho_\sigma(\vec{r}) = \sum_i n_{i\sigma} |\phi_{i\sigma}(\vec{r})|^2 \quad (2)$$

where $\phi_{i\sigma}$ are the numerical cluster spin-orbitals with occupation $n_{i\sigma}$, which are expanded on a basis of numerical atomic orbitals.

The variational method leads to the conventional secular equations, which are solved self-consistently in a three-dimensional numerical grid. A total of $\sim 24,000$ points were used for the cluster. A multipolar expansion of the charge density, centered at the nuclei of the cluster atoms, is used to construct the model potential employed in the hamiltonian of Eq. (1) [17]. The model density is fitted to the true density by a least-squares procedure; here only atom-centered spherical terms were considered, which is adequate for a compact metal.

A Mulliken-type population analysis [22], [24] was employed, to assess the contributions of the 3d, 4s and 4p orbitals to the net charges and magnetic moments μ . The latter were also calculated by integrating the spin-up and spin-down total and difference charge densities within the Wigner-Seitz spheres of the atoms. Partial densities of states (DOS) are defined by [25]:

$$D_{nl\sigma}^q(E) = \sum_i P_{nl\sigma,i}^q \frac{\delta/\pi}{(E - \varepsilon_{i\sigma})^2 + \delta^2} \quad (3)$$

where $P_{nl\sigma,i}^q$ is the Mulliken population of atomic orbital χ_{nl} of atom q in the cluster spin orbital $\phi_{i\sigma}$, and δ is the half-width of the Lorentzian functions employed to broaden the cluster levels, to simulate a continuum ($\delta = 0.136eV$ here). By summing over n, ℓ and i the local DOS of spin σ for atom q is obtained.

Hyperfine fields H_F were also computed at the Fe nucleus. For metals, the total field may be considered to a good approximation to be equal to the Fermi or contact field H_c :

$$H_c = (8/3)\pi\mu_B [\rho_\uparrow(0) - \rho_\downarrow(0)] \quad (4)$$

where μ_B is the Bohr magneton and the term in brackets is the difference between the electron density at the nucleus for spin up and spin down. The details of the calculation of H_c were given in a previous publication [26].

III Results and Discussion

a. fcc iron

Theoretical studies with band structure methods have demonstrated the existence of several magnetic states of γ -Fe [1], [2]. For smaller values of the lattice constant, the antiferromagnetic state is more stable than the ferromagnetic; for larger values the situation is inverted. Experimentally, the interatomic distances may be varied in γ -Fe particles or films by employing pressure or by using Cu-based alloys with metals such as Au and Al, which have a larger atomic radius [13].

In a previous publication, we reported calculations of H_F for fcc Fe at several interatomic distances, for the antiferromagnetic (AFM) and ferromagnetic (FM) states [26]. There it was demonstrated that the conduction electrons contribution to H_F has different sign for the AFM and FM spin configurations. This difference in sign is responsible for the large gap found experimentally in the magnitude of the hyperfine fields between these two states. Here we present some additional results of the calculations for pure fcc Fe.

Several lattice constants were considered, varying from $a=3.38\text{\AA}$ to 3.77\AA . For smaller values, as occurs in a Cu matrix, an antiferromagnetic spin arrangement is present, as was demonstrated by band structure calculations [2] and neutron diffraction measurements [4], [6]. For larger distances, the ferromagnetic spin structure prevails [2]. For the antiferromagnetic state, a structure consisting of alternating layers of up and down spins normal to the (001) direction was considered: this is represented in Fig. 1 by alternating layers of different shades. It has been shown recently that a more complex spiral spin structure is actually present [9], [27]. However, the main qualitative features of antiferromagnetism are present in our model. In all cases, the convention adopted defines the magnetic moments of the Fe atoms in the (x,y) plane as positive. Thus FM γ -Fe is represented by the cluster $\text{Fe}_{62\uparrow}$, and AFM γ -Fe by the cluster $\text{Fe}_{36\uparrow}\text{Fe}_{26\downarrow}$ (see Fig. 1).

In Table I are given the Mulliken populations and spin moments μ , as well as volume moments as defined previously. Although calculations were done for several values of the lattice constant, we include only two values in the table, a smaller value in the region of the AFM phase and a larger value in the FM region. These two distances are representative of the values found for the FM and AFM states. The local properties are presented for the innermost atoms in the cluster, which are most representative of the bulk metal. For the outer atoms, small differences are found, due to cluster-boundary effects. The table shows that volume and Mulliken moments are not very different. The 4s, 4p conduction electrons are polarized parallel to the 3d moment in the AFM case, and antiparallel in the FM structure; this has been previously related to the hyperfine fields [26]. The 3d population is near 7 in both cases. The 4p population is larger than 4s in the AFM case, the opposite being true for FM γ -Fe. The magnetic moments obtained here are in good agreement with band structure calculations [1],[2] for the FM state, and are somewhat larger for AFM.

The spin DOS (defined as spin up DOS minus spin down DOS) for the total valence states (3d, 4s, 4p) of FM γ -Fe is shown in Fig. 3 as well as the 3d-only component. We may observe in the total spin DOS in Fig. 3 oscillations at the lower (upper) band edges corresponding to the more strongly bonding (antibonding) states, that are due to the conduction (4s 4p) electrons. The 4s, 4p spin DOS showing clearly this oscillatory character in Fig. 3, is of great importance, as it is responsible for the observed long-range polarization ($> 10\text{\AA}$) in multicomponent films. These same features are present in the spin DOS of the AFM state. In Figs. 4a and 4b are plotted the total valence DOS for FM and AFM states, respectively, for spin up and spin down separately. The main difference between these two diagrams is that the spin up band for the FM state is practically entirely occupied, whereas for AFM both bands are partially occupied. The peak of the AFM spin-down band is above the Fermi level, which gives raise to a net magnetic moment.

In Figs. 5a and 5b we may see spin density maps ($\rho_{\uparrow}(\vec{r}) - \rho_{\downarrow}(\vec{r})$) in the (x,z) plane of

the cluster for FM and AFM states respectively. We notice that the point symmetry of the cluster (D_{4h}) yields spin densities that are compatible with the translational symmetry of the fcc crystal to a considerable extent. This demonstrates that the cluster is a satisfactory representation of the bulk metal. In the FM state (Fig. 5a) the spin density of the conduction electrons antiferromagnetically aligned with respect to 3d (see Table I) may be seen as dotted curves in between the atoms.

b. Coherent Fe Particle in Copper

In Table 2 are given Mulliken populations and magnetic moments for a small Fe particle in Cu represented by the cluster $\text{Fe}_{14}\text{Cu}_{48}$ (see Fig. 2). The AFM and FM states were obtained self-consistently, for the same distances as in Table 1. In the AFM configuration the particle has four atoms in the (x,y) plane with positive spin moments, and five each in the planes above and below with negative spins. Thus there is a net number of six spin down atoms in the AFM particle, represented by $(\text{Fe}_{4\uparrow}\text{Fe}_{10\downarrow})\text{Cu}_{48}$, whereas the configuration of the cluster representing the FM particle is $(\text{Fe}_{14\uparrow})\text{Cu}_{48}$.

Comparing these data with Table I, we see that there is little difference in the 3d, 4s and 4p populations of Fe in this particle relative to pure γ -Fe. Thus charge transfer from or into the Cu matrix is small. We notice that the Fe 4p populations are slightly decreased in the particle. As a consequence of the net spin mentioned above, derived from the large imbalance between the number of atoms with up and down spins in the AFM particle (4 and 10, respectively), we find an asymmetry in the magnitude of the magnetic moments of the atoms in the spin up and spin down layers.

A most interesting result is the spin polarization of the surrounding copper atoms, which is shown in Table II. For the FM particle, the 3d moments on the Cu atoms are positive, and thus aligned with the Fe 3d moments, while the 4s, 4p moments of Cu are antiparallel to the Fe 3d moment. For the AFM particle, since there are six more atoms with spin down than with spin up, the Cu atoms align their 3d moments parallel to the majority spin down 3d of Fe, and 4s and 4p of Cu have positive spins. The volume moments of Cu have the same sign as the 3d contribution since the volume integration is performed in a region restricted to the vicinity of the atomic nucleus where the compact 3d orbital is dominant.

This result is entirely in agreement with recent findings on Co/Cu and Fe/Cu multilayers, using magnetic circular X-ray dichroism at the K edge of copper [28],[29]. This sophisticated technique allows measurement of the spin polarization on the Cu atoms, and to distinguish between 3d and 4p states. According to these experimental measurements, the 3d electrons of Cu are polarized parallel to the 3d moment of Fe, whereas the 4p of Cu are antiparallel. Since the experiments were made on an Fe-Cu multilayer system with different geometry from that of the particle treated in the present work, we conclude that the direction of the orbital polarization on Cu induced by Fe is an intrinsic property of those atoms.

Figures 6a and 6b illustrate the spin polarization of the Fe particle in copper and the copper response. In Fig. 6a is shown the spin density map for the AFM particle in copper in the (x,z) plane. We see the spins of the compact 3d electrons of copper

aligned parallel to the (majority) spin down Fe atoms. The positive spin density of the conduction electrons is not seen because it is weak and diffuse. However, we see a small positive spin region of the copper atoms which are nearest to the Fe atoms with positive moments. In Fig. 6b, the spin density map for the FM particle in copper is shown. In the compact region around the Cu nuclei corresponding to the 3d moments, the spin density is positive, aligned with the Fe atoms 3d moments. The spin density of the conduction electrons, which is negative both for Cu and Fe, is partially visible as the dotted lines between the atoms.

c. Influence of Substitutional Al

In constructing Fe precipitates in Cu alloys with Al, with the purpose of increasing the lattice constant due to the larger atomic radius of Al, it was verified that a fraction of the Al atoms penetrated the Fe precipitates [13]. This experimental result motivated our investigation of the influence of Al impurities in γ -Fe and in the Fe precipitate in copper.

The two innermost Fe atoms on the z axis in the clusters representing γ -Fe and the Fe particle in Cu (see Figs. 1 and 2) were substituted by Al, to assess the influence of Al in the electronic and magnetic properties of the bulk metal and the particle. We chose these atomic positions to preserve the point symmetry (D_{4h}), for computational reasons. Thus in the AFM case, Al is substituting for two Fe atoms with negative moments. The configurations of the clusters representing bulk γ -Fe with substitutional Al are $\text{Fe}_{36\uparrow}\text{Fe}_{24\downarrow}\text{Al}_2$ for AFM, and $\text{Fe}_{60\uparrow}\text{Al}_2$ for FM. The configurations of the clusters representing the Fe particle with substitutional Al in Cu are $(\text{Fe}_{4\uparrow}\text{Fe}_{8\downarrow}\text{Al}_2)\text{Cu}_{48}$ for AFM, and $(\text{Fe}_{12\uparrow}\text{Al}_2)\text{Cu}_{48}$ for FM.

In Table III are displayed net charges and magnetic moments for AFM and FM bulk γ -Fe with Al ($\text{Fe}_{60}\text{Al}_2$), and for the FM Fe particle with Al in Cu, $(\text{Fe}_{12}\text{Al}_2)\text{Cu}_{48}$. The reason for not including the AFM Fe/Al particle in Cu in the table is that this configuration did not converge in the self-consistent procedure. As the iterations evolved, the antiparallel spins on Fe became parallel, and the FM state resulted. Thus we conclude that Al atoms destabilize the AFM particle in copper.

That Al has a destabilizing effect on the AFM state of γ -Fe was also verified for the case of Al impurities in pure γ -Fe. The calculation did not reach full self-consistency due to oscillations in the potential during the iterations, the magnetic moments being given with an uncertainty of $\pm 0.02\mu_B$. Another indication is the magnitude of the spin moments on the neighbor Fe atoms in the same plane as Al (not shown in Table III), which decreased considerably ($\mu = -0.05\mu_B$) as compared to pure AFM. On the other hand, the spin up moments increase, as may be seen in Table III ($1.61\mu_B$, as compared to $1.50\mu_B$ in Table I). In Table III we see also that the Al moments are negative, i.e. of spin opposite to the positive Fe spins on the (x,y) plane.

Figure 7a illustrates the spin distribution in the (x,z) plane for bulk Fe AFM with Al represented by $\text{Fe}_{36\uparrow}\text{Fe}_{24\downarrow}\text{Al}_2$. The diffuse negative (3s, 3p) spin density of the Al atoms is attracted by the Fe atoms with spin up moments and repelled by spin down. Accordingly, in the case of FM γ -Fe with two Al atoms ($\text{Fe}_{60\uparrow}\text{Al}_2$), as seen in Fig. 7b for the (x,z) plane, we observe that the Al negative spin density fills all the space between the nearby Fe atoms.

The calculated reduction of the Fe 3d magnetic moment due to the presence of neighbor

Al atoms in FM γ -Fe is entirely analogous to the case of Al impurities in FM bcc Fe (as shown by DVM cluster calculations [21]), as is the decrease in the magnitude of the conduction electron antiparallel moments (compare tables III and I). This weakening of the FM iron moment by hybridization with Al 3s, 3p states reaches its limit in the total suppression of (experimental) moment in the case of dilute Fe in Al. As we have shown [19], the local lattice relaxation plays a vital part in the collapse of the local Fe moment, so further lattice-relaxation studies of small particles may show significant effects on net particle magnetization. The calculated increase of Fe moment in the AFM state is an interesting consequence of the relative size (weaker) of Al-Fe versus Fe-Fe interactions.

In Fig. 8 is drawn the spin density distribution of the FM Fe particle with Al in Cu ($\text{Fe}_{12}\text{Al}_2$) Cu_{48} . There is clearly seen the compact 3d spin density around the Cu nuclei, of the same sign as the Fe atoms spin density, and the extended negative (3s,3p) spin density of the two Al atoms. The Cu spin distribution and moment is hardly changed relative to the pure FM γ -Fe particle in copper.

In Table III are also given the charges on Fe and Al. There is a pronounced charge transfer from Al to the nearest-neighbor Fe. The magnitude of Mulliken and volume charges differ substantially, due to the diffuse nature of the valence electron density of Al.

d. Magnetic Hyperfine Fields

In Table IV are given the values of the calculated hyperfine fields H_F at the Fe nucleus. Values given are for the innermost Fe atoms on the (x,y) plane (see Figs. 1 and 2). As has been described in a previous report [26], the core contribution to H_F of γ -Fe is negative in all cases, whereas the conduction electron contribution is positive for AFM and negative for FM, mainly due to the different signs of the polarization of the (4s,4p) electrons in the two states. These general features are maintained for the Fe particle in the copper environment, as well as in the presence of Al.

For the AFM state, the magnitude of H_F is increased by the presence of the Al neighbors, due to the increase in the core contribution. This is explained by the increase in the 3d moment resulting from the presence of the Al neighbors (compare Tables I and III), since the core H_F is proportional to the 3d moment. The core H_F is always negative, resulting from a delicate balance of polarization of the 1s, 2s and 3s core electrons by the 3d spin. However, if H_F were calculated at a spin down Fe site neighbor to Al, the trend would be the opposite, since the 3d moment there is decreased, as described earlier. Actually, the tendency in the neighborhood of Al is the transformation AFM \rightarrow FM by increase of the magnitude of the spin up Fe moments and decrease of spin down.

For FM Fe, the magnitude of H_F is decreased by the presence of Al, due to a decrease in $\mu(3d)$ of Fe. This situation is the same as encountered for hyperfine fields of Al alloys of bcc Fe [21].

The Fe particle in copper in the AFM configuration presents a large imbalance in the magnitudes of the Fe moments for positive and negative spins, as shown in Table II. This is reflected in different values of H_F , one larger and one smaller than for pure γ -Fe. The smaller value, corresponding to the spin up layer, is shown in Table IV. We may notice also a much larger value of the positive conduction electron contribution, due

to an increase in the 4s polarization. For FM γ -Fe, the copper environment causes an increase in the 3d moment, which is reflected in the increase of the core H_F . However, the conduction electrons H_F has its magnitude decreased considerably due to the decrease of the polarization of the (4s,4p) electrons antiparallel to Fe 3d (see Table II; in fact, the 4s magnetic moment as calculated by the Mulliken analysis has even changed sign). The magnitude of the total H_F is thus considerably decreased.

Finally, the presence of the two Al atoms in the FM particle in Cu affects only the core H_F , whose magnitude falls along with the decrease of the Fe 3d moment. Thus the total H_F has its magnitude decreased further.

Mössbauer experiments on AFM γ -Fe precipitates in CuAl result in hyperfine-field distribution curves that show a low-field maximum and a high-field tail which becomes more pronounced with increasing Al concentration [13]. By applying a strong external field, the peak was identified as due to AFM γ -Fe and the tail to FM. According to the results obtained with the present calculations, we interpret the presence of this “tail” of high-field values as due to the influence of Al impurities, which penetrate the Fe precipitates and disrupt locally the AFM spin arrangement transforming into ferromagnetic γ -Fe clusters with much higher field magnitudes.

IV Conclusions

The present calculations for γ -Fe in the AFM and FM configurations have shown that the 62-atoms cubic cluster is an adequate representation to describe magnetic properties of the bulk. Densities of states give a correct description of the magnetic moment formation, and spin-density maps, showing adequate translational symmetry, illustrate the spin distribution within the solid. Calculations for a 14-atom γ -Fe particle surrounded by 48 copper atoms show the influence of Cu on the Fe moments in the AFM and FM cases. An important result obtained is the spin polarization of the Cu atoms, which is shown to be parallel to the 3d spins of Fe for Cu 3d, and antiparallel for Cu(4s,4p). This result is the same as obtained very recently for Fe/Cu multilayers with magnetic circular dichroism experiments [29]. The presence of Al substituting for Fe was found to disrupt the AFM spin arrangement: for the AFM γ -Fe particle in copper, the presence of two Al atoms resulted in non-convergence for the self-consistent potential, indicative of the instability of that state. In pure AFM γ -Fe the two Al impurities caused a tendency to local ferromagnetic arrangement. Al substitution in FM γ -Fe causes a reduction in the 3d moment of the Fe neighbors; this same result has been reported for bcc Fe with Al impurities [21]. Finally, the influence of the Cu environment and Al impurities in the hyperfine field of Fe has been assessed: for FM Fe, both decrease the magnitude of H_F , and for AFM the situation is more complex.

Acknowledgements

Calculations were performed at the Cray YMP of the Supercomputing Center of the Universidade Federal do Rio Grande do Sul. The authors thank Cassio Magnino and Luiz Marcelo Oliveira for the computer graphs. The work of DEE was support in part

by the National Science Foundation, under U.S. - Brazil cooperative program Grant no. INT-9202608 and the MRL program, at the Materials Research Center of Northwestern University, under award no. DMR-9120521.

100
100
100
100
100
100
100
100
100
100

Figure Captions

- Fig. 1** – 62-atom cluster representing fcc iron. Spheres of different shades are used to show the alternating layers of up and down spins of the AFM phase. Lighter shade represents Fe atoms with positive magnetic moments, according to our convention.
- Fig. 2** – Cluster representing a cubic particle of iron with 14 atoms in the fcc structure, surrounded by copper atoms. Darker shade spheres represent Fe.
- Fig. 3** – Spin density of states (defined as spin-up DOS minus spin-down DOS) of the total valence (3d+4s+4p) states of FM γ -Fe; partial spin DOS for 3d; partial spin DOS for (4s+4p).
- Fig. 4a** – Valence (3d+4s+4p) DOS for FM γ -Fe.
- Fig. 4b** – Valence (3d+4s+4p) DOS for AFM γ -Fe.
- Fig. 5a** – Spin density contours ($\rho_{\uparrow}(\vec{r}) - \rho_{\downarrow}(\vec{r})$) for FM γ -Fe in the (x,z) plane. Contours are from -0.01 to $+0.01$ e/au³ with intervals of 0.001 e/au³. Full lines are positive values.
- Fig. 5b** – Spin density contours for AFM γ -Fe in the (x,z) plane. Contours are from -0.01 to $+0.01$ e/au³ with intervals of 0.001 e/au³. Full lines are positive values.
- Fig. 6a** – Spin density contours for AFM γ -Fe particle surrounded by copper, in the (x,z) plane. Contour specifications as in Figs. 9 and 10.
- Fig. 6b** – Spin density contours for FM γ -Fe particle surrounded by copper, in the (x,z) plane. Contour specifications as in Figs. 9 and 10.
- Fig. 7a** – Spin density contours for AFM γ -Fe in the (x,z) plane with two Al on the z axis, above and below the (x,y) plane. Contour specifications as in previous figures.
- Fig. 7b** – Spin density contours for FM γ -Fe in the (x,z) plane with two Al on the z axis, above and below the (x,y) plane. Contour specifications as in previous figures.
- Fig. 8** – Spin density contours for FM γ -Fe particle surrounded by Cu in the (x,z) plane with two Al on the z axis, above and below the (x,y) plane. Contour specifications as in previous figures.

Table Captions

- Table I** – Mulliken populations and spin magnetic moments for AFM and FM states of γ -Fe. Lattice constant “a” and Wigner-Seitz radius “ r_s ” are given in a.u. (0.5292 Å). Cluster for AFM is Fe₃₆ \uparrow Fe₂₆ \downarrow and for FM is Fe₆₂ \uparrow .
- a) For the interior Fe atoms of cluster in (x,y) plane; due to diffuse overlapping charge distributions, net Mulliken charges of individual atoms are not zero.

Table II - Mulliken populations and spin magnetic moments for AFM and FM γ -Fe particles surrounded by copper. Clusters are $(\text{Fe}_{4\uparrow}\text{Fe}_{10\downarrow})\text{Cu}_{48}$ for AFM, and $\text{Fe}_{14\uparrow}\text{Cu}_{48}$ for FM. Signs of spin moments are given according to the convention adopted, in which Fe atoms in (x,y) plane have positive spins.

a) For the innermost Fe atoms (spin \uparrow in the (x,y) plane and spin \downarrow in the z axis).

Table III - Mulliken populations, charges and spin magnetic moments for AFM and FM γ -Fe with Al substitutional impurities, and for the FM particle in Cu with substitutional Al impurities. Signs of spin moments are given according to the convention adopted, in which Fe atoms in (x,y) plane have positive spins.

a) For the interior Fe atoms in the (x,y) plane.

b) Substituting the 2 innermost Fe atoms in the z axis.

Table IV - Hyperfine fields (in kOe) for FM and AFM γ -Fe and particles. Calculated at the interior Fe atoms in the (x,y) plane (positive spin moment).

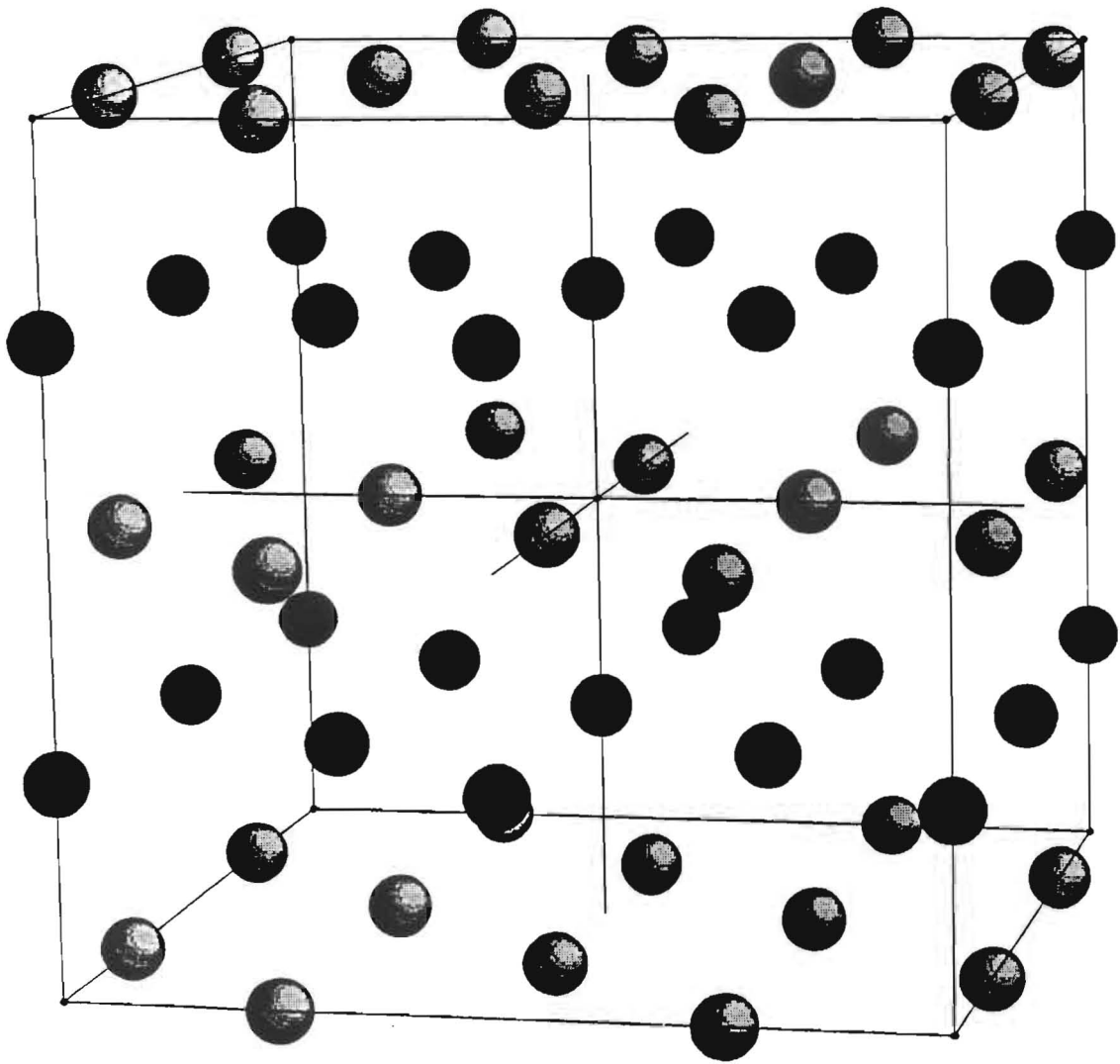


Fig. 1

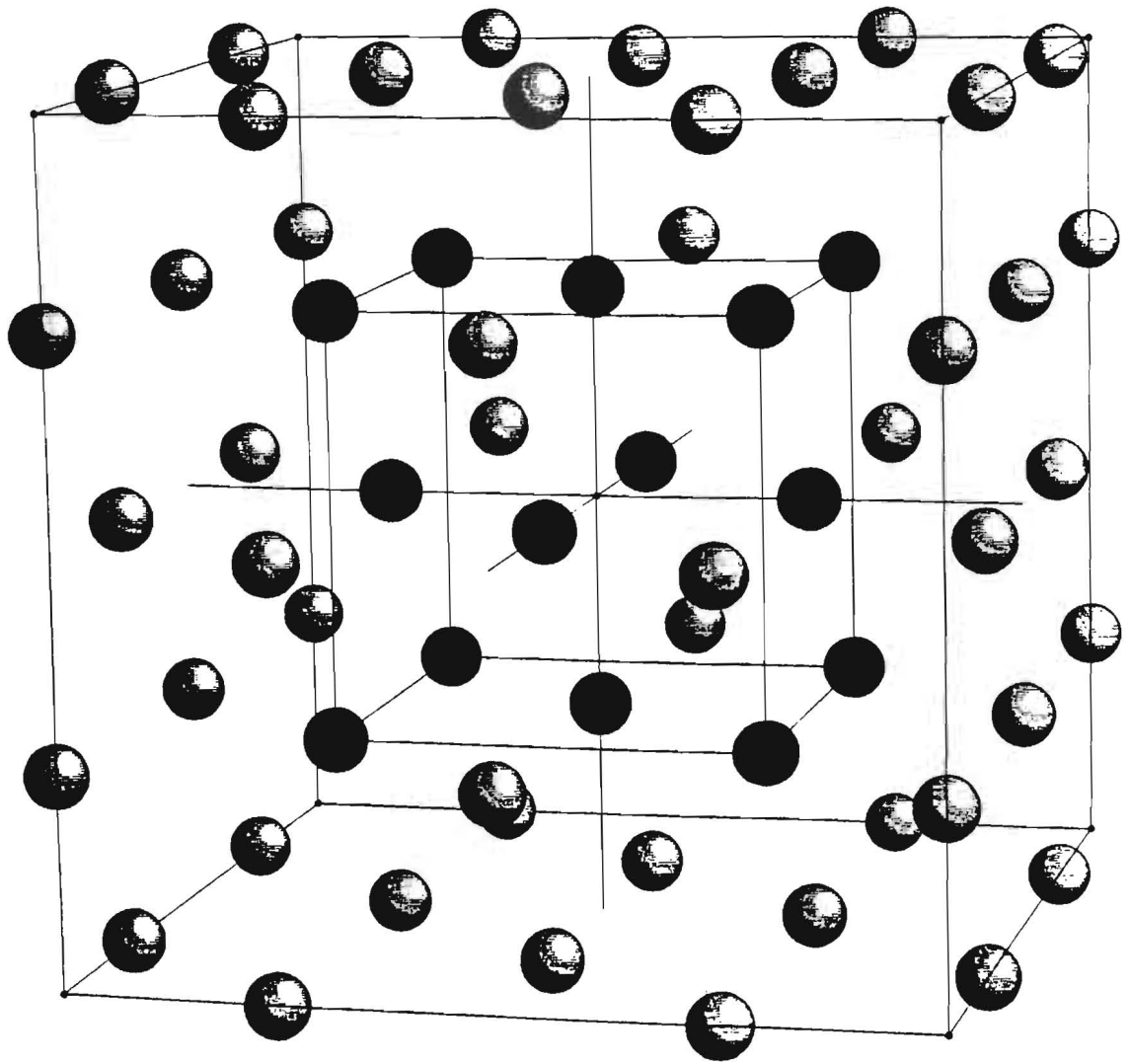


Fig. 2

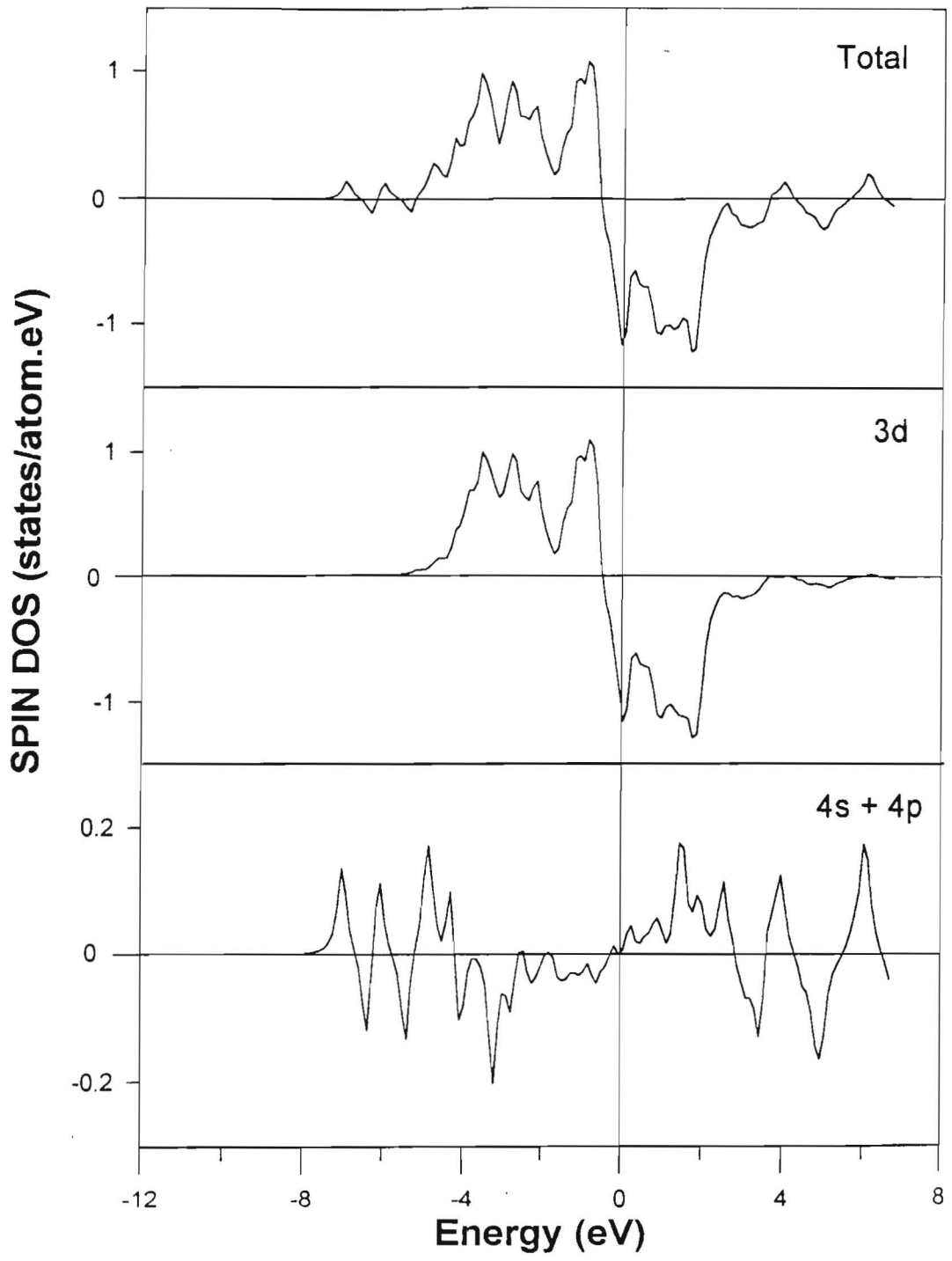


Fig. 3

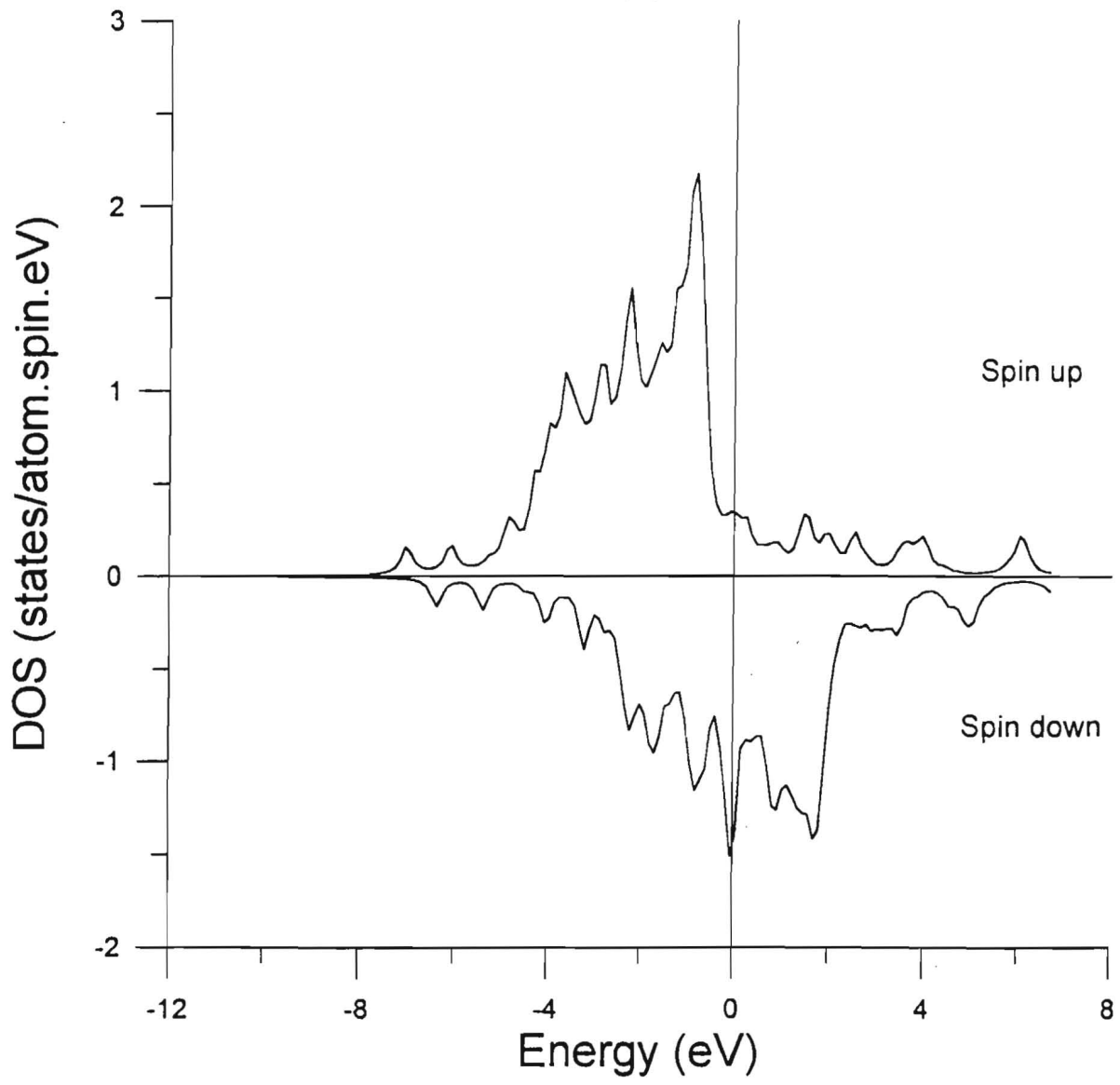


Fig. 4a

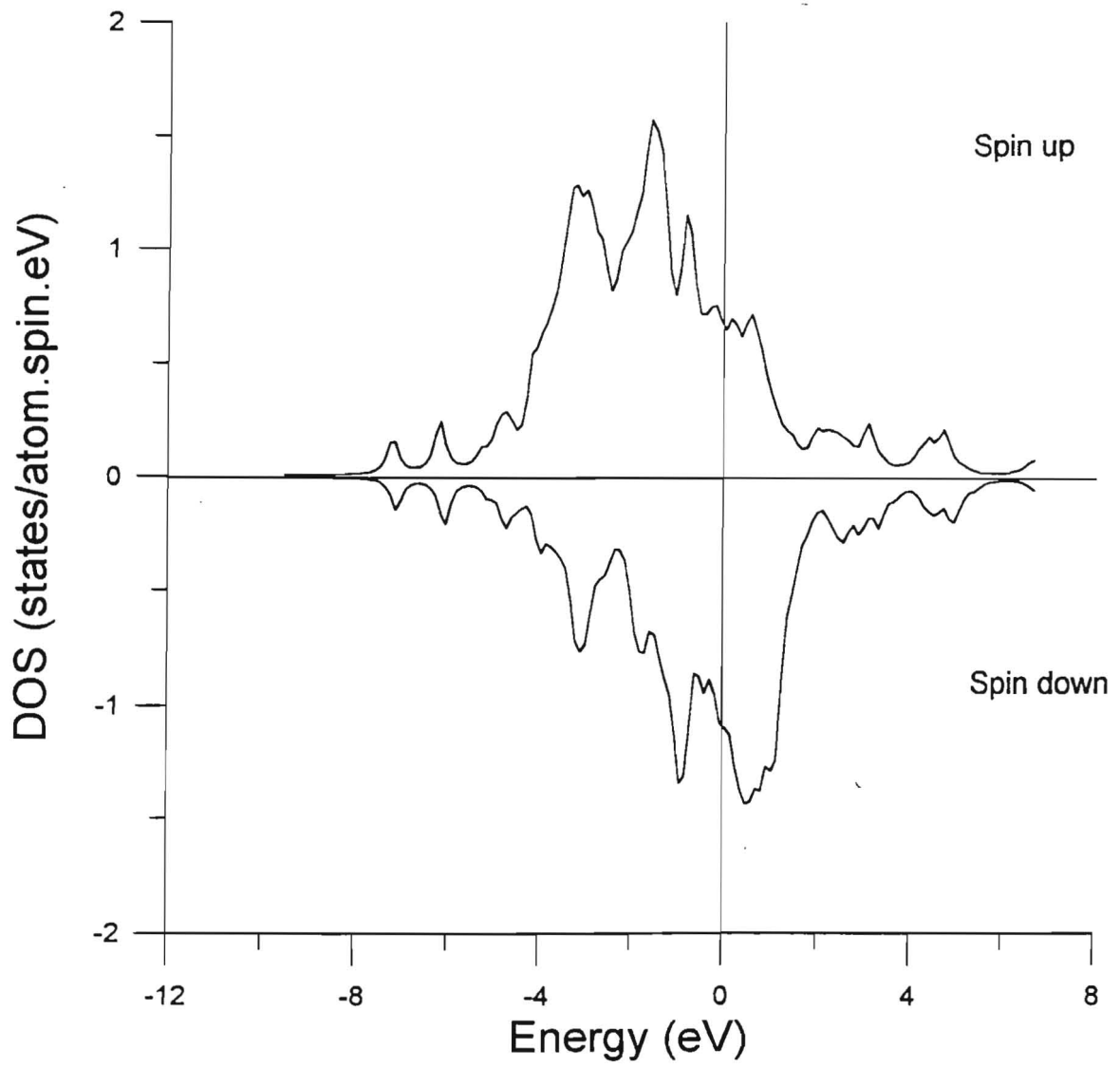


Fig. 4b

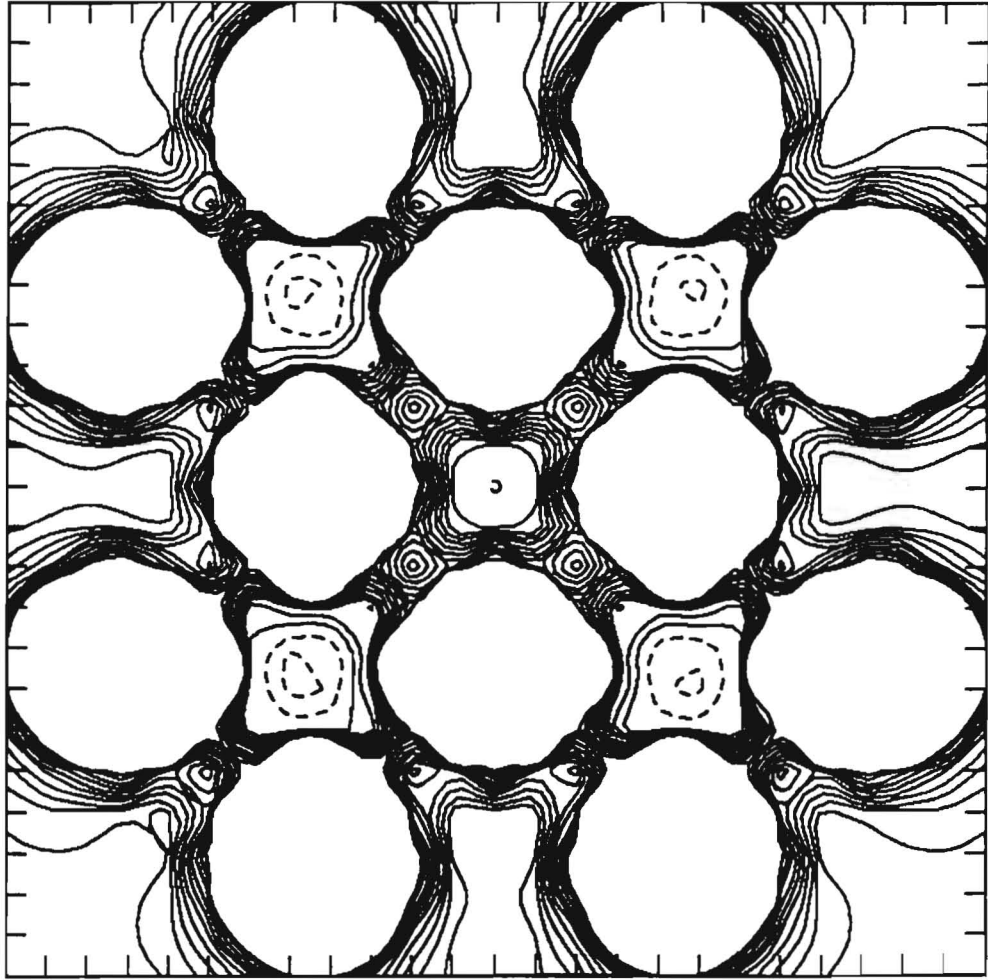


Fig. 5a

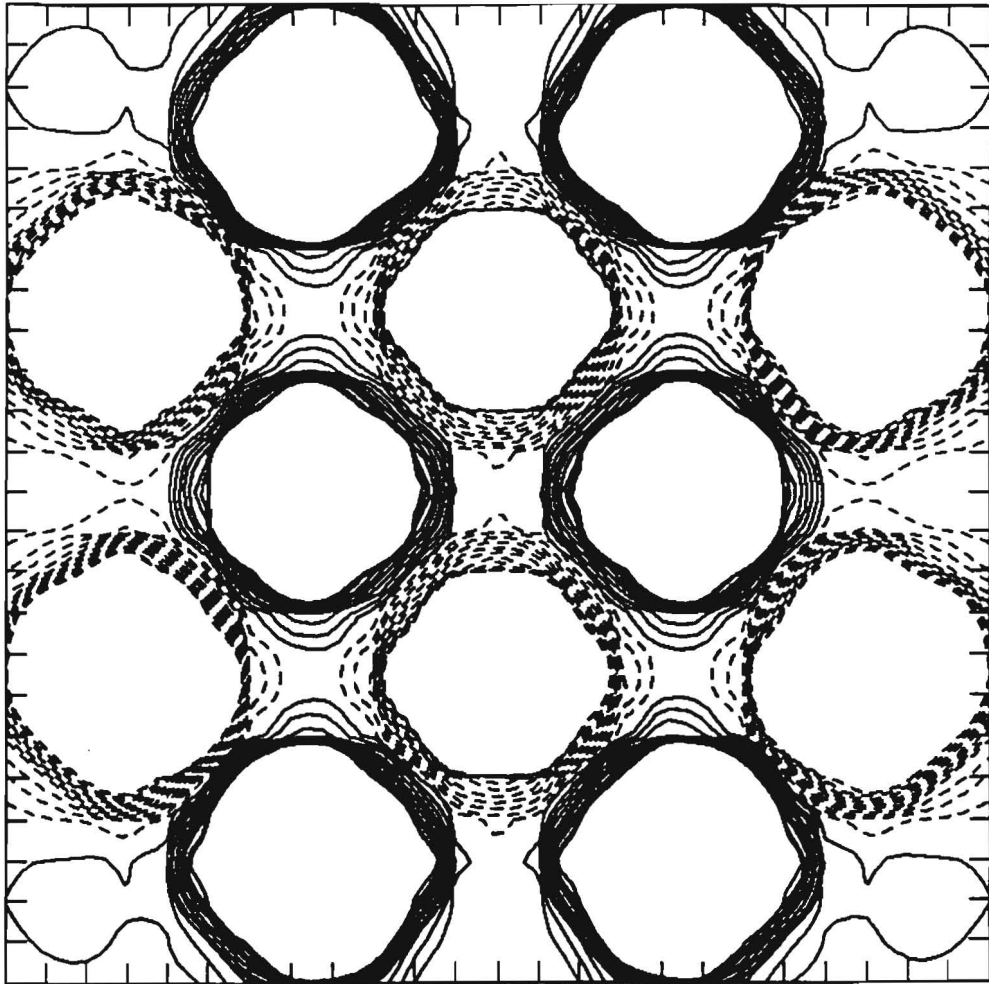


Fig. 5b

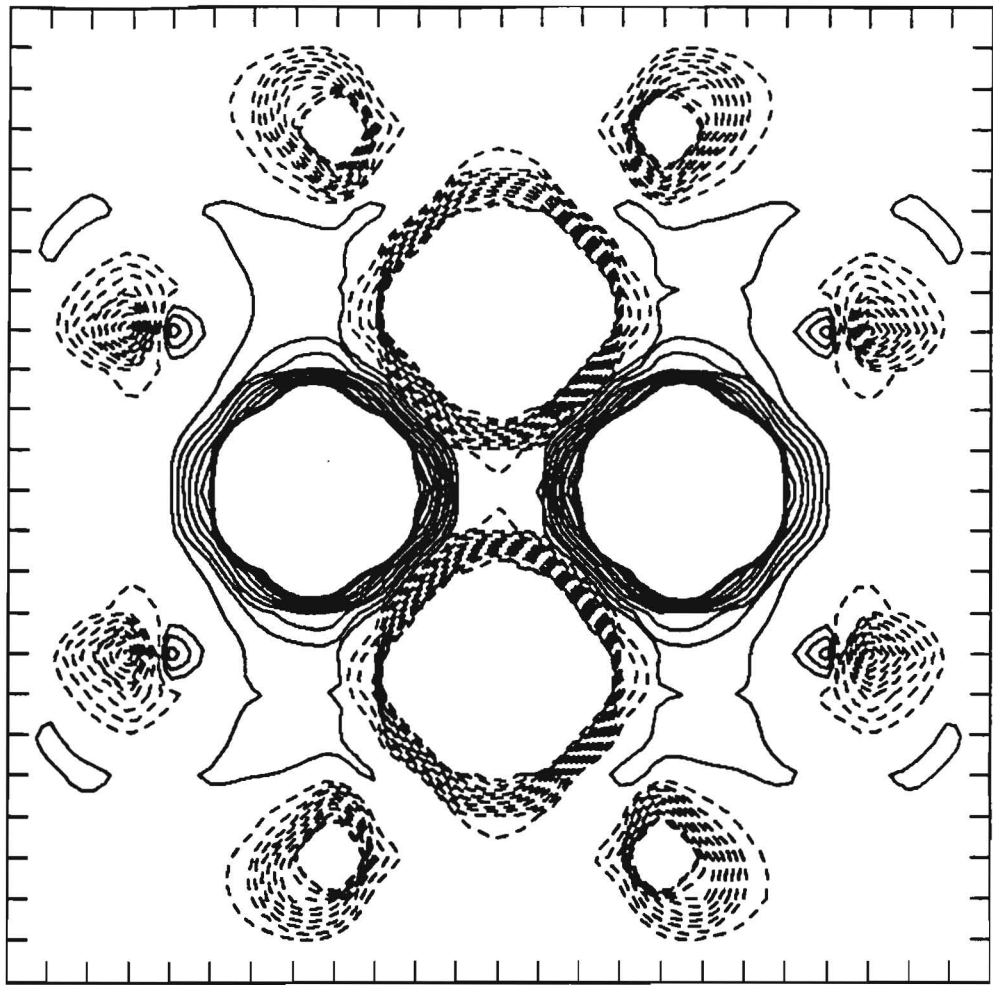


Fig. 6a

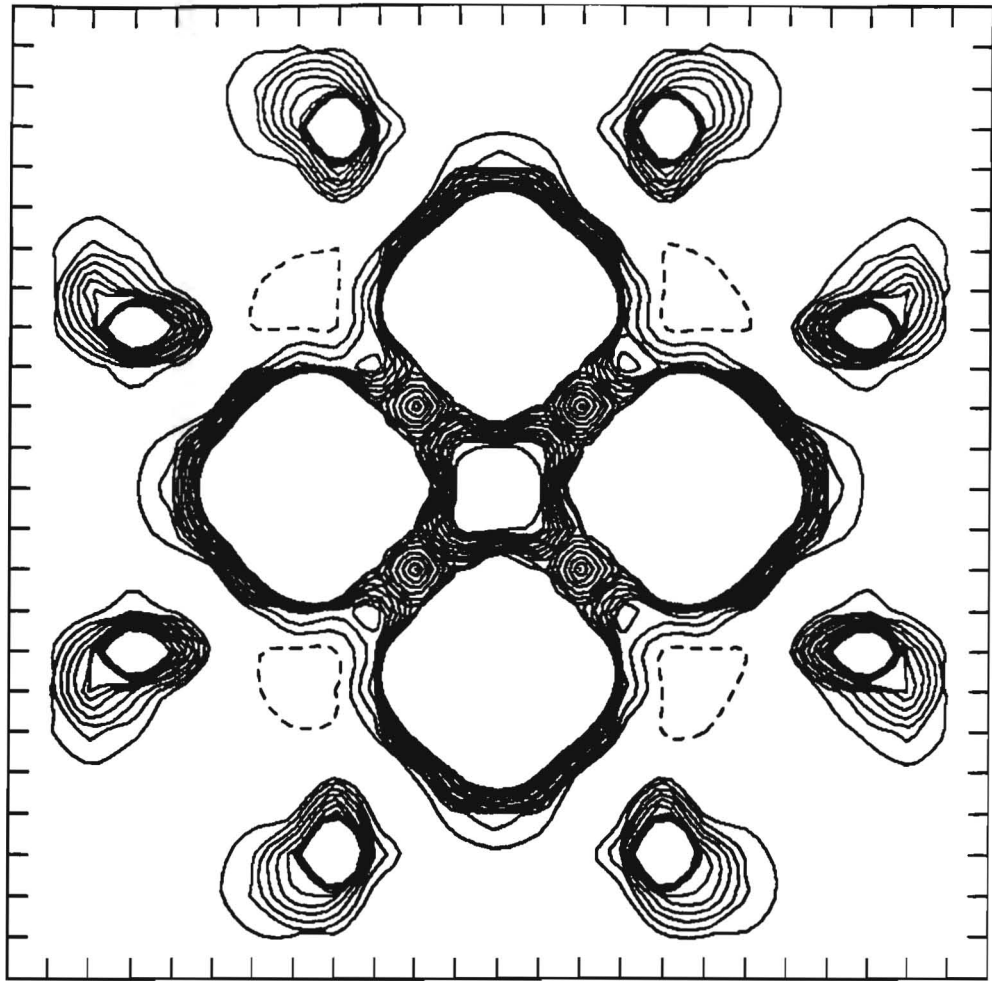


Fig. 6b

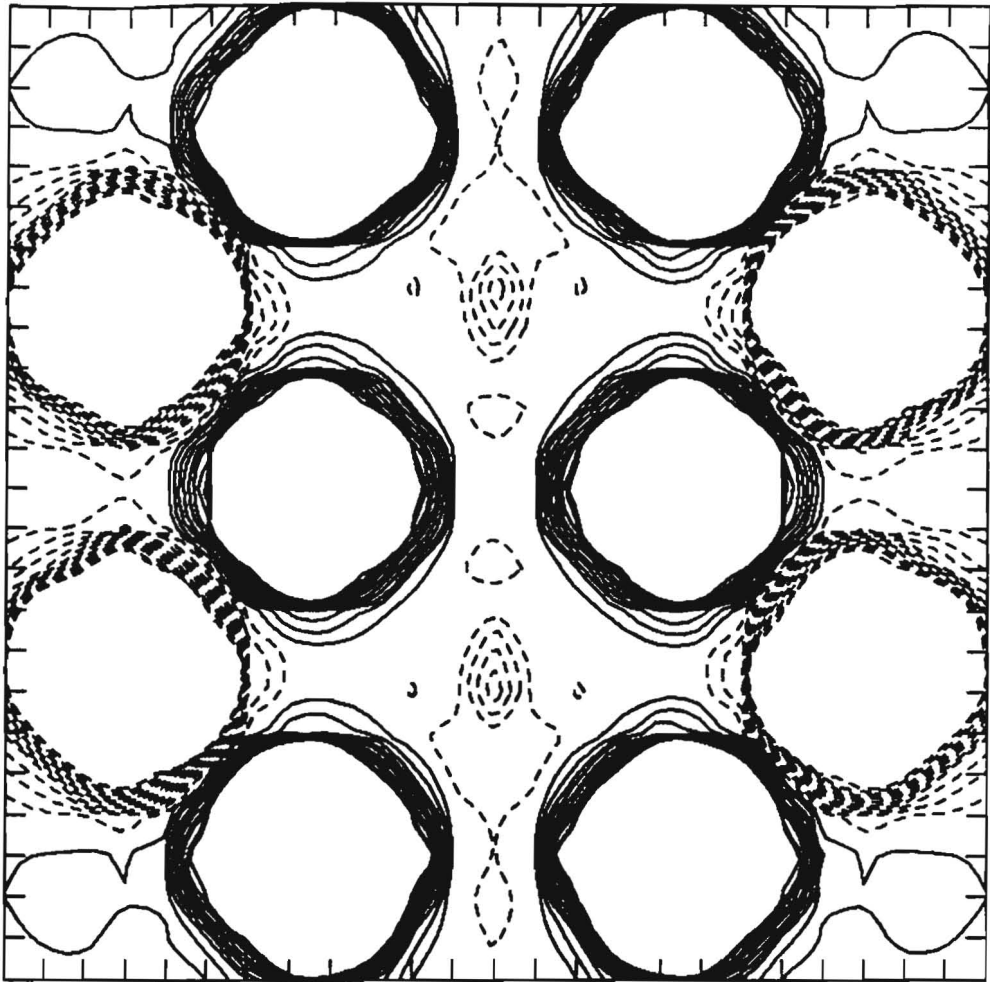


Fig. 7a

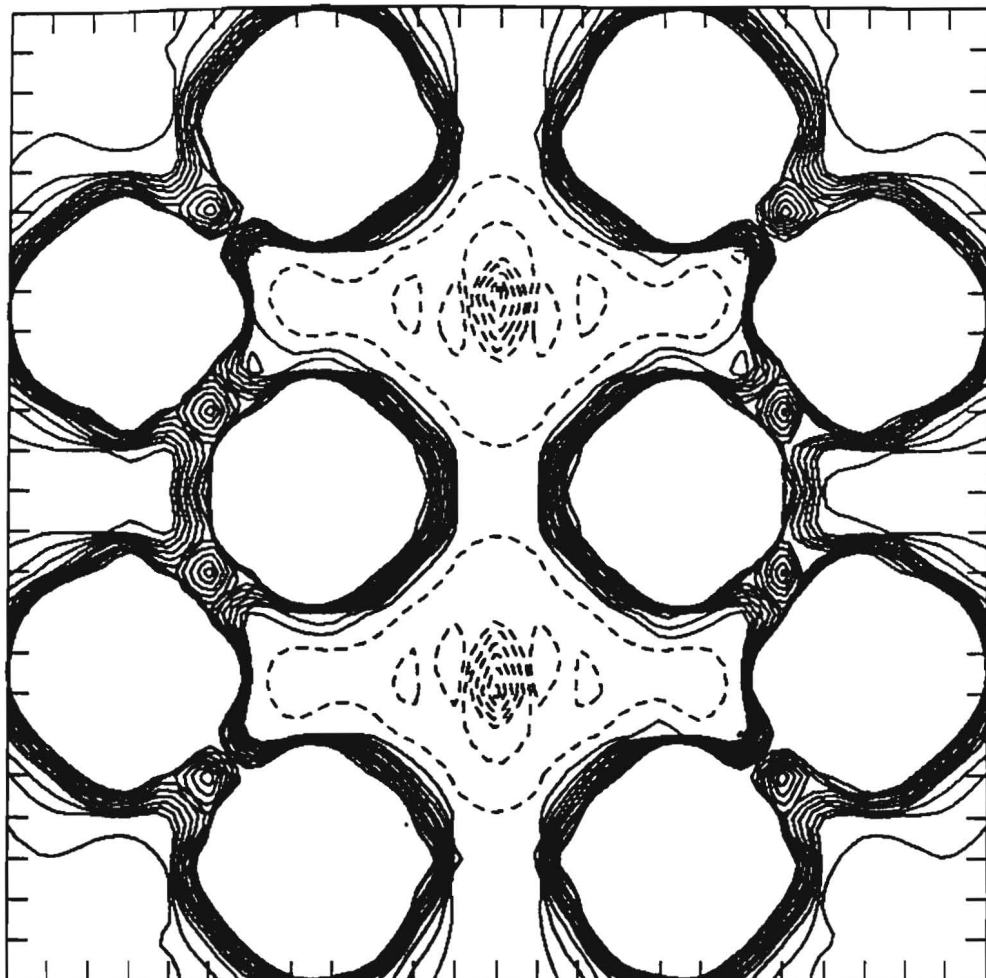


Fig. 7b

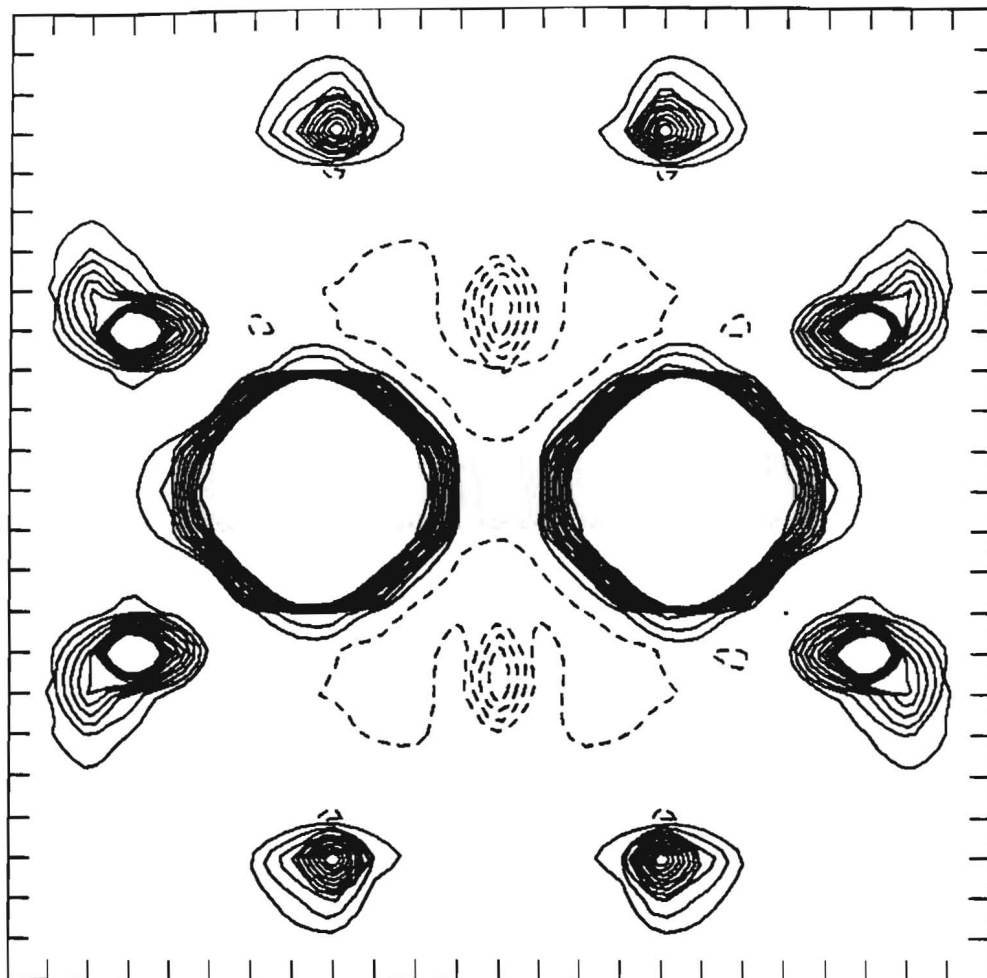


Fig. 8

TABLE I

| | Mulliken Populations ^{a)} | | Spin magnetic moments (μ_B) ^{a)} | | |
|---|---------------------------------------|------|---|-------|--------|
| | | | Mulliken | | volume |
| AFM a=6.73au r _s =2.63au | 3d | 7.10 | 3d | 1.41 | 1.37 |
| | 4s | 0.39 | 4s | 0.04 | |
| | 4p | 0.56 | 4p | 0.05 | |
| | Total | | Total | 1.50 | |
| FM a=6.96au r _s =2.72au | 3d | 7.06 | 3d | 2.50 | 2.41 |
| | 4s | 0.53 | 4s | -0.01 | |
| | 4p | 0.43 | 4p | -0.05 | |
| | Total | | Total | 2.44 | |

TABLE II

| Fe populations ^{a)} | | Fe magnetic moments (μ_B) ^{a)} | | Cu magnetic moments (μ_B) | |
|------------------------------|---------------------------|---|-----------------|---------------------------------|--------|
| | | Mulliken | Volume | Mulliken | Volume |
| AFM $r_s=2.63\text{au}$ | spin \uparrow 3d 7.18 | 3d 1.21 | 1.18 | | |
| | 4s 0.42 | 4s 0.06 | | | |
| | 4p 0.42 | 4p <u>0.07</u> | | | |
| | | Total 1.34 | | | |
| | spin \downarrow 3d 7.09 | 3d -1.86 | -1.81 | 3d -0.04 | -0.03 |
| 4s 0.34 | 4s -0.04 | 4s +0.01 | | | |
| 4p 0.39 | 4p <u>-0.03</u> | 4p <u>+0.02</u> | | | |
| | Total -1.93 | Total -0.01 | | | |
| FM $r_s=2.72\text{au}$ | 3d 7.05 | 3d 2.56 | 3d +0.04 | | |
| | 4s 0.54 | 4s 0.01 | 4s -0.02 | | |
| | 4p 0.35 | 4p <u>-0.03</u> | 4p <u>-0.02</u> | | |
| | Total 2.54 | 2.50 | Total 0.0 | +0.01 | |

TABLE III

| | Cluster | Fe charge ^{a)} | Al charge | Fe magnetic moments (μ_B) ^{a)} | | Al magnetic moments (μ_B) ^{b)} | | Cu magnetic moments (μ_B) | |
|---|---|------------------------------|----------------|---|--------|---|--------|--|--------|
| | | | | Mulliken | Volume | Mulliken | Volume | Mulliken | Volume |
| γ -Fe+2(Al) AFM $r_s=2.63\text{au}$ | $\text{Fe}_{36\uparrow}\text{Fe}_{24\downarrow}\text{Al}_2$ | Mulliken:0.0 Volume:-0.17 | +0.22 +0.43 | 3d 1.53 4s 0.04 4p 0.04 Total 1.61 | 1.50 | 3s -0.01 3p -0.18 Total -0.19 | -0.06 | - | - |
| γ -Fe+2(Al) FM $r_s=2.72\text{au}$ | $\text{Fe}_{60\uparrow}\text{Al}_2$ | Mulliken:0.0 Volume:-0.16 | +0.22 +0.43 | 3d 2.33 4s -0.01 4p -0.03 Total 2.29 | 2.24 | 3s -0.05 3p -0.30 Total -0.35 | -0.12 | - | - |
| Fe particle in Cu+2(Al) FM $r_s=2.72\text{au}$ | $(\text{Fe}_{12\uparrow}\text{Al}_2)\text{Cu}_{48}$ | Mulliken:0.0 Volume:-0.07 | +0.24 +0.51 | 3d 2.39 4s 0.01 4p -0.01 Total 2.39 | 2.33 | 3s -0.05 3p -0.22 Total -0.27 | -0.08 | 3d 0.03 4s -0.02 4p -0.02 Total -0.01 | +0.01 |

TABLE IV

| | | Cluster | $H_c^{cond.}$ | H_c^{core} | $H_c^{tot} \cong H_F$ |
|------------------------------|---|---|---------------|--------------|-----------------------|
| AFM $r_s = 2.63\text{au}$ | $\left\{ \begin{array}{l} \gamma - \text{Fe} \\ \gamma - \text{Fe} + 2(\text{Al}) \\ \gamma - \text{Fe in Cu} \end{array} \right.$ | $\text{Fe}_{36\uparrow}\text{Fe}_{26\downarrow}$ | +44 | -157 | -113 |
| | | $\text{Fe}_{36\uparrow}\text{Fe}_{24\downarrow}\text{Al}_2$ | +35 | -171 | -136 |
| | | $(\text{Fe}_{4\uparrow}\text{Fe}_{10\downarrow})\text{Cu}_{48}$ | +86 | -130 | -44 |
| FM $r_s = 2.72\text{au}$ | $\left\{ \begin{array}{l} \gamma - \text{Fe} \\ \gamma - \text{Fe} + 2(\text{Al}) \\ \gamma - \text{Fe in Cu} \\ \gamma - \text{Fe in Cu} + 2(\text{Al}) \end{array} \right.$ | $\text{Fe}_{62\uparrow}$ | -59 | -288 | -347 |
| | | $\text{Fe}_{60\uparrow}\text{Al}_2$ | -60 | -268 | -328 |
| | | $(\text{Fe}_{14\uparrow})\text{Cu}_{48}$ | -23 | -296 | -319 |
| | | $(\text{Fe}_{12\uparrow}\text{Al}_2)\text{Cu}_{48}$ | -23 | -275 | -298 |

References

- [1] J. Kübler, *Phys. Lett.* **81A**, 81 (1981).
 - [2] C.S. Wang, B.M. Klein and H. Krakauer, *Phys. Rev. Letters* **54**, 1852 (1985).
 - [3] E.F. Wassermann, *Physica Scripta* **T25**, 209 (1989).
 - [4] S.A. Abrahams, L. Guttman and J.S. Kasper, *Phys. Rev.* **127**, 2052 (1962).
 - [5] U. Gonser, C.J. Meechan, A.H. Muir and H. Wiedersich, *J. Appl. Phys.* **34**, 2373 (1963).
 - [6] G.J. Johanson, M.B. McGire and D.A. Wheeler, *Phys. Rev.* **B1**, 3208 (1970).
 - [7] B. Window, *Philos. Mag.* **26**, 681 (1972).
 - [8] P. Ehrhart, B. Schönfeld, H.H. Ettwig and W. Pepperhoff, *J. Magn. Magn. Mater.* **22**, 79 (1980).
 - [9] A. Onodera, Y. Tsunoda, N. Kunitomi, O.A. Pringle, R.M. Nicklow and R.M. Moon, *Phys. Rev. B*, **50**, 3532 (1994).
 - [10] U. Gonser, K. Krischel and S. Nasu, *J. Magn. Magn. Mater.* **15-18**, 1145 (1980).
 - [11] T. Ezawa, W.A.A. Macedo, U. Glos, W. Keune, K.P. Schletz and U. Kirschbaum, *Physica B* **161**, 281 (1989).
 - [12] W.A.A. Macedo and W. Keune, *Phys. Rev. Lett.* **61**, 475 (1988).
 - [13] W. Keune, T. Ezawa, W.A.A. Macedo, U. Glos, K.P. Schletz and U. Kirschbaum, *Physica B* **161**, 269 (1989).
 - [14] C.L. Fu and A.J. Freeman, *Phys. Rev. B* **35**, 925 (1987).
 - [15] D.E. Ellis, *Int. J. Quant. Chem. Suppl.* **2**, 35 (1968).
 - [16] D.E. Ellis and G.S. Painter, *Phys. Rev. B* **2**, 2887 (1970).
 - [17] B. Delley and D.E. Ellis, *J. Chem. Phys.* **76**, 1949 (1982).
 - [18] D. Guenzburger and D.E. Ellis, *Phys. Rev. B* **36**, 6971 (1987); *Phys. Rev. B* **31**, 93 (1985).
 - [19] D. Guenzburger and D.E. Ellis, *Phys. Rev. Letters* **67**, 3832 (1991).
 - [20] D. Guenzburger and D.E. Ellis, *Phys. Rev. B* **49**, 6004 (1994).
 - [21] H. Chacham, E. Galvão da Silva, D. Guenzburger and D.E. Ellis, *Phys. Rev. B* **35**, 1602 (1987).
-

- [22] D.E. Ellis, J. Guo and J.J. Low in "Quantum Chemistry Approaches to Chemisorption and Heterogeneous Catalysis", ed. F. Ruette, Kluwer, Amsterdam (1992), pag. 69.
- [23] U. von Barth and L. Hedin, *J. Phys. C* **5**, 1629 (1972).
- [24] R.S. Mulliken, *J. Chem. Phys.* **23**, 1853 (1955); *ibid*, pag. 1841.
- [25] P.-L. Cao, D.E. Ellis and A.J. Freeman, *Phys. Rev. B* **25**, 2124 (1982).
- [26] D. Guenzburger and D.E. Ellis, *Phys. Rev. B* **51**, 12519 (1995).
- [27] Y. Tsunoda, N. Kunitomi and R.M. Nicklow, *J. Phys. F* **17**, 2447 (1987).
- [28] M.G. Samant, J. Stöhr, S.S.P. Parkin, G.A. Held, B.D. Hermsmeier, F. Herman, M. van Schilfgaarde, L.-C. Duda, D.C. Mancini, N. Wassdahl and R. Nakajima, *Phys. Rev. Letters* **72**, 1112 (1994).
- [29] S. Pizzini, A. Fontaine, C. Giorgetti, E. Dartyge, J.-F. Bobo, M. Piecuch and F. Baudalet, *Phys. Rev. Letters* **74**, 1470 (1995).

NOTAS DE FÍSICA é uma pré-publicação de trabalho original em Física.
Pedidos de cópias desta publicação devem ser enviados aos autores ou ao:

Centro Brasileiro de Pesquisas Físicas
Área de Publicações
Rua Dr. Xavier Sigaud, 150 - 4^o andar
22290-180 - Rio de Janeiro, RJ
Brasil

NOTAS DE FÍSICA is a preprint of original unpublished works in Physics.
Requests for copies of these reports should be addressed to:

Centro Brasileiro de Pesquisas Físicas
Área de Publicações
Rua Dr. Xavier Sigaud, 150 - 4^o andar
22290-180 - Rio de Janeiro, RJ
Brazil